RESEARCH PAPER

Nanosphere dispersion on a large glass substrate by low dose ion implantation for localized surface plasmon resonance

Xiaodong Zhou · Kai Yu Liu · Nan Zhang ·
Dong-Hwan Kim · Christina Tan

Abstract Dispersing nanospheres on a large glass substrate is the key to fabricate noble metal nanostructures for localized surface plasmon resonance through dispersed nanosphere lithography. This article reports that by modifying the glass surface with low dose ion implantation and successively dip coating the surface with poly(diallyldimethyl ammonium chloride) (PDDA), polystyrene or silica nanospheres can be dispersed on a large glass substrate. Investigation shows that several kinds of ions, such as silicon, boron, argon, and arsenic, can improve the nanosphere dispersion on glass, attributed to the ion bombardment-caused silicon increment. Ion implantation imposes no surface roughness or optical loss to the glass substrate, thus this method is suitable for localized surface plasmon resonance application. Experiments show silicon ion implantation can best disperse the nanospheres. For the gold nanostructures obtained by obliquely evaporating 30 nm of gold film onto the polystyrene nanospheres, which are dispersed on a silicon ion implanted glass substrate, a localized surface plasmon resonance sensitivity of 242 nm/RIU is achieved.

X. Zhou (✉) · N. Zhang · C. Tan
Institute of Materials Research and Engineering, A*STAR
(Agency for Science, Technology and Research),
3 Research Link, Singapore 117602, Singapore
e-mail: donna-zhou@imre.a-star.edu.sg

N. Zhang
e-mail: n-zhang@imre.a-star.edu.sg

C. Tan
e-mail: yl-tan@imre.a-star.edu.sg

K. Y. Liu
School of Electrical and Electronic Engineering, Nanyang
Technological University, 50 Nanyang Avenue,
Singapore 639798, Singapore
e-mail: liuky@yahoo.com

D.-H. Kim
Division of Bioengineering, School of Chemical and
Biomedical Engineering, Nanyang Technological
University, Singapore 637457, Singapore
e-mail: dhkim@ntu.edu.sg

Introduction

In a recent decade, localized surface plasmon resonance (LSPR) (Endo et al. 2005; Li et al. 2010; Willets and Duyne 2007; Zhao et al. 2006), which utilizes the resonance between the electrons in noble metal nanoparticles and incident light, has been developed to detect the refractive index changes adjacent to these nanoparticles. LSPR is similar to surface plasmon resonance (SPR) (Homola et al. 1999; Homola 2003), which is a well-established technology and requires some complicated optical setup to detect the analytes through biological interfaces on a noble metal film. However, LSPR

displays many advantages over its counterpart SPR, for instance, the electromagnetic field decay length of LSPR is reduced from 150–200 nm to 5–15 nm and the electromagnetic field intensity is 10 times enhanced within the decay length; the peak wavelength of LSPR is tunable by the size and shape of the nanoparticles; and most importantly, its detection is simplified by measuring the transmission spectrum of the nanoparticles, rather than requiring prism, grating, or waveguide in SPR to enhance the momentum of the light.

Nanoparticle fabrication plays a key role in realizing a highly sensitive LSPR biosensor, and the nanoparticles are desired to be identical, reproducible on a relatively large area with low fabrication cost. The nanoparticles used in LSPR can be fabricated by the means such as nanosphere lithography (NSL), synthesis, e-beam lithography, and nanoimprinting, among which NSL is the most cost-effective. Nanostructures fabricated by NSL possess sharp corners and render high LSPR sensitivity and tenability, and their LSPR detections have been demonstrated with nanotriangles (Willets and Duyne 2007; Zhao et al. 2006) and nanocaps (Endo et al. 2005; Li et al. 2010) fabricated by closely packed nanospheres (Yang et al. 2006; Zhang et al. 2007), and nanocrescents (Bukasov and Shumaker-Parry 2007; Rochholz et al. 2007; Shumaker-Parry et al. 2005) and nanoholes (Gao et al. 2007; Prikulis et al. 2004; Xiang et al. 2010) fabricated by dispersed nanosphere lithography. Closely packed NSL is prone to generate defects for a critical length greater than 10–100 μm. For dispersed NSL, the nanospheres tend to huddle on a glass substrate and only disperse in a small area. It has been reported that polystyrene nanospheres can be dispersed in a large area of square centimeter on some substrates including titanium oxide (Hanarp et al. 2003), PMMA photoresist (Fredriksson et al. 2007), silicon (Zhou et al. 2008), and amorphous silicon-modified glass surface (Zhou et al. 2009) and they were achieved by chemical treatment as well as some surface modification technologies. Since LSPR is measured by optical transmission, titanium oxide will increase the reflected optical loss in addition to the cost increment. In the results reported by Fredriksson et al. (2007), PMMA was a photoresist for nanopatterning; in order to get rid of PMMA and only leave gold nanostructures on the glass substrate, at least two more fabrication steps, including the O₂ plasma PMMA etching and gold lift-off, were added compared with dispersing the nanospheres directly on a glass substrate, and the metal lift-off in nanoscale is relatively difficult.

Polystyrene nanospheres can be well dispersed on silicon substrate by dip coating poly(diallyldimethyl ammonium chloride) (PDDA) prior to the drop coating of the nanospheres (Zhou et al. 2008), due to the fact that the positive charges provided by the PDDA coating and silicon substrate can cancel out the negative charges of the polystyrene nanospheres and disperse them. However, no nanospheres were found on PDDA-coated glass substrate after rinsing when the same process was applied (Zhou et al. 2009). A method of modifying the glass surface with a layer of deposited amorphous silicon was reported, but it caused some optical loss due to the refractive index mismatch between the amorphous silicon and glass (Zhou et al. 2009).

This article reports that by introducing a new technique which uses low dose ion implantation to modify the glass substrate, polystyrene, or silica nanospheres can be successfully dispersed on the glass surface with the use of PDDA. This method does not change the optical properties of the glass for LSPR measurements, and is compatible with semiconductor fabrication process and thus mass producible. The experimental results indicate that any kind of ions can be implanted into the glass to disperse the nanospheres, while silicon produces the most satisfactory result.

Compared with the reported methods of dispersing the polystyrene nanospheres on TiO₂, PMMA, and silicon, this is the first reported method to disperse the nanospheres on glass substrate without changing its optical properties. Dispersion of the nanospheres on TiO₂, PMMA, or silicon is purely based on the wet chemical treatment; while this method is a combination of physical treatment (ion implantation to physically modify the glass surface) and wet chemical (PDDA to introduce positive electrostatic charges) treatment. Since only one kind of chemical (PDDA) is used in the process, the process is simple and its repeatability and reproducibility are high over a large glass substrate (2 cm × 2 cm). Its disadvantage is that with only one kind of chemical used, through experiments we found out that it is unable to adjust the interdistance of the nanospheres by changing the concentration of the nanosphere

solution. By introducing more than one kind of chemical, such as using the combination of PDDA/PSS(polysodium 4-styrenesulfonate)/ACH (aluminum chloride hydroxide) (Hanarp et al. 2003) and modifying the ratio of different chemicals, the interdistance of the nanospheres can be varied; however, additional wet chemical processing steps might influence its reproducibility.

Experiments

The nanospheres used in the experiments were 170, 260, and 360 nm diameter polystyrene nanospheres and 500 nm diameter silica nanospheres, purchased from Duke Scientific Ltd as 10% suspension in water. PDDA with a medium molecular weight of 20 wt% in water was purchased from Aldrich.

4″ Pyrex 7740 glass wafers were implanted in Varian EHP-200 ion implanter at implantation energy of 5 keV, with doses of 1E13, 1E14, and 1E15/cm^2 for silicon ion implantation, and 1E14/cm^2 for boron, argon, and arsenic ion implantations, respectively. Subsequently, the wafers were diced into 2 cm × 2 cm chips by a Disco dicing saw, and each chip was cleaned by sonication in acetone for 3 min, rinsed and dried. The implantation depths of the ions in the samples were measured by secondary ion mass spectrometer (SIMS) ION-TOF SIMS IV, and the implantation depth of the silicon ions at 5 keV is simulated with the software Stopping and Range of Ions in Matter (SRIM). Another two pieces of glass in the size of a few millimeters, chopped from the glass wafer, were sputtered in X-ray photoelectron spectroscopy (XPS) VG ESCALAB 220I-XL with two kinds of sputtered energy: 3 keV for 90 min and 1 keV for 45 min, respectively, at an argon dose of 1E15/cm^2. The silicon percentage on the glass surface is measured by the same XPS machine. After the ion implantations and XPS sputtering, the roughness of sample surfaces was inspected by an atomic force microscope (AFM) from Multimode-Digital Instruments.

To check the dispersion of the nanospheres on the glass samples, the ion implanted glass substrate was dip coated with a 1:5 diluted PDDA solution for 30 s. After rinsing with deionized water and drying, the substrate was drop coated with 1 mL diluted nanosphere solution, rinsed with deionized water to get rid of the excessive nanospheres, and dried by nitrogen gas. The nanospheres on the glass substrate were observed by JEOL JSM7400F field emission gun scanning electron microscope (FEGSEM).

For the LSPR measurement, gold was evaporated onto the glass substrate by a R-Dec thermal evaporator at a rate of 0.5–0.7 Å/s, and the LSPR spectra were taken by an Ocean Optics USB2000-UV–Vis optical fiber spectrometer around the wavelength range of 350–900 nm.

Discussions

Dispersion of the nanospheres and its mechanism

Without PDDA treatment, polystyrene nanospheres are mostly huddled together and dispersed only in a small area of the glass substrate, as the SEM picture shown in Fig. 1a. With PDDA treatment, the situation is even worse, that no nanospheres remain on the glass substrate after rinsing (Zhou et al. 2009). However, in our experiments, it is found that by processing the glass substrates with low dose ion implantation prior to the PDDA treatment, nanospheres can be dispersed on the glass substrate. SEM images of the substrates treated with silicon implantation at the doses of 1E13, 1E14, and 1E15/cm^2 all revealed uniformly dispersed nanospheres on the substrate, at a density of 4/μm^2 for 170 nm diameter nanospheres. A representative SEM picture of these samples is presented in Fig. 1b, and a typical dose of 1E14/cm^2 is selected for other ion implantation experiments. Figure 1b has the same magnification and area size of Fig. 1a, thus the dispersion of the nanospheres is prominent in Fig. 1b. Further experiments show that for a glass substrate of 2 cm × 2 cm in square, polystyrene nanospheres with diameters of 170, 260, and 360 nm as well as silica nanospheres with diameter of 500 nm could be well dispersed allover the substrate including the corners, and the results were highly repeatable.

Besides silicon ion implantation, other ion species were also investigated by implanting the glass substrate at a dose of 1E14/cm^2 to disperse the nanospheres with PDDA treatment. It was found that the implantations of boron, argon, and arsenic ions could also disperse the nanospheres on the glass substrate as presented in Fig. 1c–e, but the results were not as good as silicon ion implantation. In the
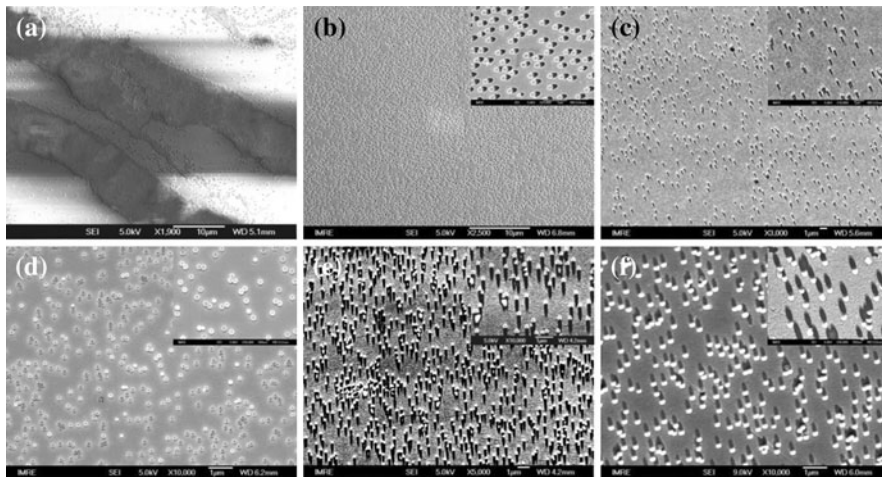
Fig. 1 SEM images showing the dispersion of 170 nm diameter polystyrene nanospheres on various glass substrates. **a** shows the nanospheres on a bare glass substrate without PDDA treatment. **b**–**f** present nanospheres dispersed with PDDA treatment on glass substrates modified with silicon, boron, argon, arsenic implantations, and argon sputter in XPS, respectively, with magnified images in the *insets*. **a** and **d** were taken prior to gold evaporation, while others were with gold evaporated at an oblique angle, where the shadows of the gold film on the nanospheres can be seen

process of dispersing the nanospheres with PDDA, silicon on the glass surface plays the key role, as the negative charges of the nanospheres and the positive charges of PDDA cancel each other on a surface with silicon, which impedes the nanospheres from aggregation (Zhou et al. 2009). A possible explanation for this surface silicon accumulation by ion implantation is that the implanted ions strike the glass surface, damage the surface lattice, and break some Si–O binding of the glass. The oxygen ions might either stay on the glass surface, or escape out of the surface as oxygen has less surface-binding energy than silicon; the unbounded silicon ions are left on the glass surface and help to disperse the nanospheres. Silicon implantation is the most effective in dispersing the nanospheres, because it has extra implanted silicon ions accumulated on the surface besides the ones generated by implantation bombardment.

To testify the above assumption, two glass substrates were processed in VG ESCALAB 220I-XL XPS machine with sputtered energies of 3 keV for 90 min and 1 keV for 45 min, respectively, at an argon dose of $1E15/cm^2$. Both samples can well disperse the polystyrene nanospheres, and the nanosphere dispersion result of a sample processed at 1 keV for 45 min is shown in Fig. 1f. This indicates that just as for boron, argon, and arsenic implantations, the bombardment of the argon in XPS breaks the band between Si

and O on the glass surface and leaves silicon on the glass surface. For comparison, another glass substrate was argon sputtered in a reactive ion etching (RIE) machine, the nanospheres cannot be dispersed on this surface, due to the fact that the argon plasma in the RIE machine is not strong enough to break the Si–O band on the glass surface. Since XPS machine can only fit in samples of a few millimeters in size, it is not feasible to be used for modifying the surface of a relatively large glass substrate.

The nanospheres of 170 nm in diameter in Fig. 1b have an average density of $4/\mu m^2$, in Fig. 1c–f, this density does not vary a lot for the same size polystyrene nanospheres. This is because PDDA and silicon on the glass surface only generate a fixed ion force to disperse the nanospheres, that even on a silicon wafer surface, the same kind of nanospheres dispersed by PDDA exhibit a similar density (Zhou et al. 2008), disregarding the concentration of the nanosphere solution. However, larger nanospheres have a lower particle density, for example, the dispersed density of 360 and 500 nm diameter nanospheres is about $2/\mu m^2$, as reported before (Zhou et al. 2009).

At the low implantation dose of $1E14/cm^2$, the plateau of the implanted silicon and boron ions cannot be discerned in their SIMS plots, due to the abundance of silicon and boron in Pyrex 7740 glass.
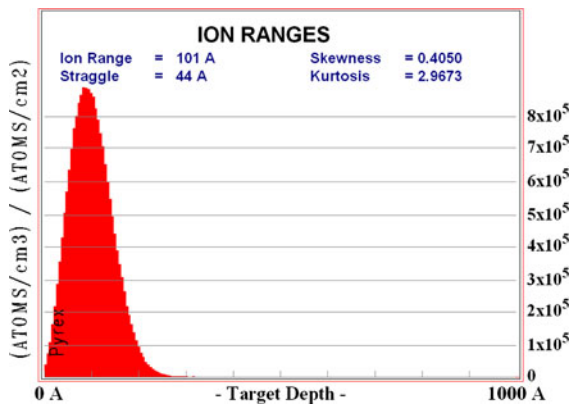
Fig. 2 Implantation profile of silicon ions into the glass at implantation energy of 5kev. The profile exhibits a plateau at 10 nm, and the ion concentration is calculated by multiplying the value on the right vertical axis by the dose

Thus, the silicon ions implanted at 5 keV were simulated by SRIM software as drawn in Fig. 2, which presents an implantation depth of 10 nm. This manifests that the ions implanted into the glass substrate are superficial. Due to the atom weights of silicon (14), boron (5), argon (18), and arsenic (33), boron ions have a deeper implantation depth than that of silicon, whereas the implantation depths of argon and arsenic ions are implanted shallower. This explains why argon and arsenic ions seem to be more effective than boron ions in dispersing the nanospheres as shown in Fig. 1, because these ions are bombarded closer to the glass surface and are more effective for obtaining silicon on the glass surface.

Since the silicon on the surface of the substrate determines the nanosphere dispersion effect, XPS analyses were performed for some samples before and after XPS sputtering and silicon implantation, with results summarized in Table 1. In Table 1, the silicon on the glass surface has a higher overall percentage after silicon implantation or XPS sputtering, but the ratio of silicon/oxygen follows no obvious trend, which means the oxygen is not escaping the glass surface after the S–O bind breakage. Table 1 shows a strong carbon reduction after XPS sputtering for samples 1 and 2, and a moderate carbon reduction after silicon implantation for sample 3. Samples 1 and 2 were analyzed with XPS right after the XPS sputtering, while sample 3 was kept in the lab for a long time after silicon implantation. This indicates that the organic contaminations on the surface of the treated samples are reduced by the XPS sputtering and ion implantation. Although a clean surface facilitates the effective electrical interactions among the PDDA, silicon, and nanospheres, however, this should be a minor contribution to the nanosphere dispersion, because there was no obvious difference on the dispersion results of samples 1 to 3.

Surface roughness and optical loss

As the bombardment of ion implantation or XPS sputtering might damage the glass surface, these samples were examined by AFM to measure the surface morphology. The average roughness (R_a) values taken from AFM for the bare glass, the glass substrates after silicon, boron, argon, and arsenic ion implantations and after XPS argon sputtering were 0.966, 0.820, 1.065, 1.332, 1.092, 8.342 nm, respectively, with their AFM images presented in Fig. 3. The results indicate no surface unevenness was introduced by ion implantations compared with the

Table 1 XPS measurements of the glass substrates surface without and with XPS sputtering (at an argon dose of 1E15/cm^2) and silicon implantation (at 5 keV with a dose of 1E14/cm^2)

| Sample	XPS analyzed percentage					Ratio of Si2p/O1s
	O1s	Si2p	C1s	Ca2p	Sc2p	
XPS sample 1						
Before XPS Ar sputtering	45.87	24.53	28.85	0.75	0	0.535
After XPS Ar sputtering at 3 keV for 90 min	64.94	33.34	1.72	0	0	0.513
XPS sample 2						
Before XPS Ar sputtering	35.73	18.41	44.75	1.11	0	0.515
After XPS Ar sputtering at 1 keV for 45 min	57.91	39.43	0	2.66	0	0.681
Sample 3 after silicon implation	53.98	28.50	17.14	0	0.39	0.528
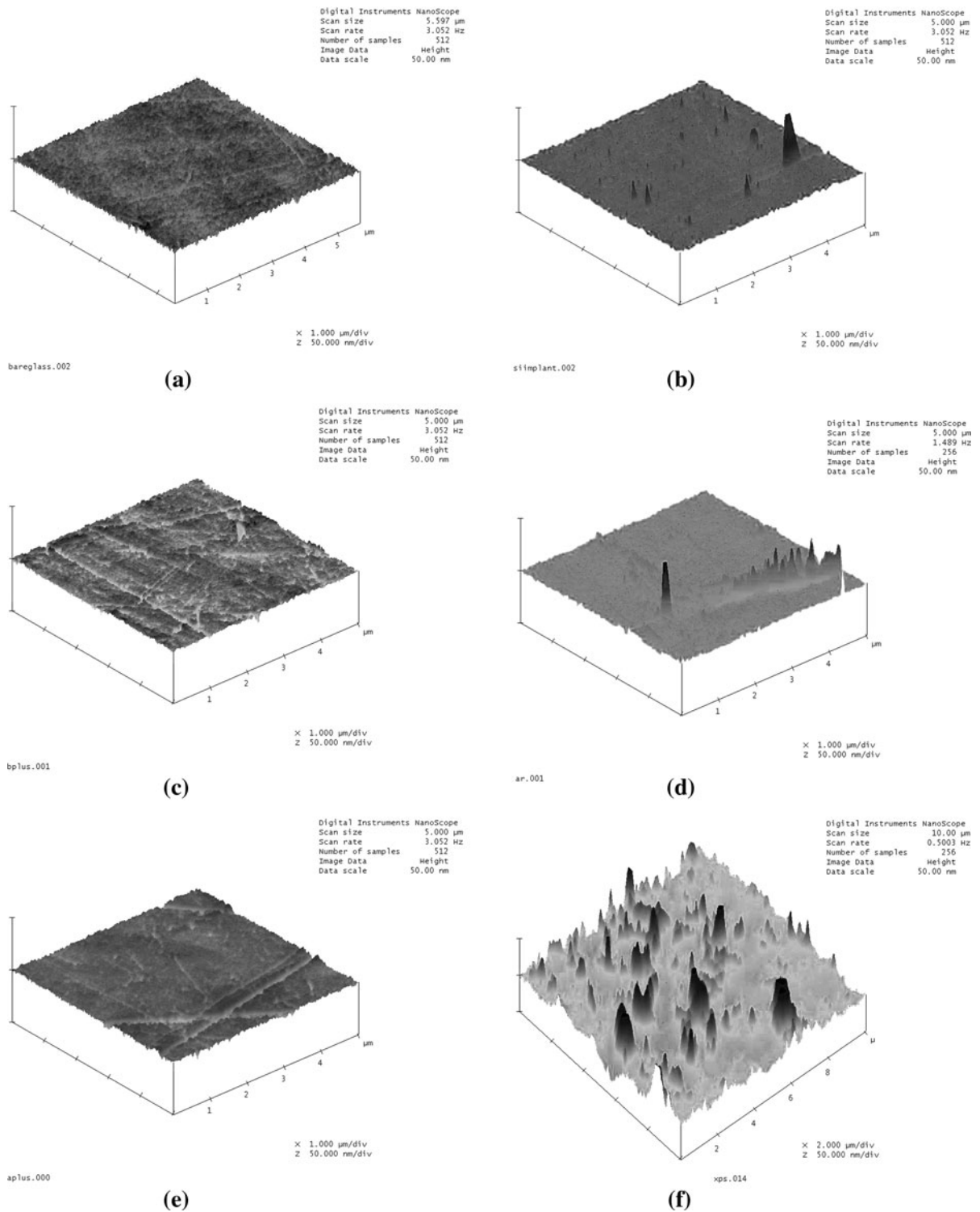
Fig. 3 Roughness of the various glass surfaces viewed under AFM. **a** Bare glass wafer and surfaces modified with ion implantations of **b** silicon, **c** boron, **d** argon, **e** arsenic, and **f** XPS sputtering of argon. **a**–**e** are scanned in a 5 μm × 5 μm area, **f** is in a 10 μm × 10 μm area. The vertical scale of these pictures is 50 nm. Although not shown in this figure, the average roughness (R_a) values of **a**–**f** are 0.966, 0.820, 1.065, 1.332, 1.092, and 8.342 nm, respectively

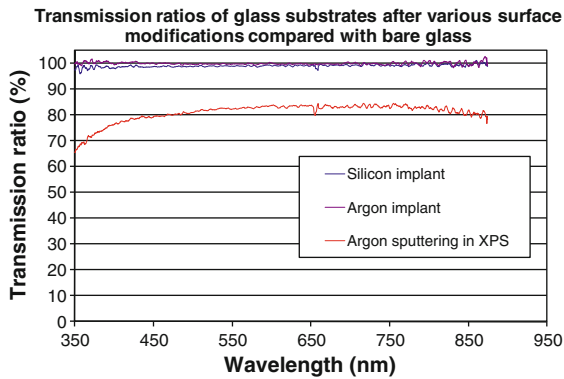**Transmission ratios of glass substrates after various surface modifications compared with bare glass**

Fig. 4 Relative transmission ratios of the glass substrates treated with silicon implantation, argon ion implantations, and argon sputtering in a XPS machine, compared with a bare glass substrate

original bare glass surface, while XPS sputtering brings obvious roughness on glass surface due to its high energy bombardment.

In order to evaluate the optical loss of the substrate caused by these surface modifications, optical spectra of these samples were measured with an Ocean Optics optical fiber spectrometer. The optical transmission spectrum of a sample is decided by the substrate material, wavelength band of the light source, and the detector's light response. It is more straightforward to compare the transmission ratio of a sample to a bare glass substrate, thus the transmission ratios of the samples to a bare glass substrate are plotted in Fig. 4, over the wavelength range of 350–900 nm. Since ion implantation causes insensible loss in light transmission, this ratio is close to 100%, while the optical transparency for the XPS-sputtered sample is only 83%. This transmission ratio is directly related with the flatness of the samples after the surface modification treatment: the ion implanted substrates have almost the same surface roughness as the untreated bare glass under AFM, thus induce no extra optical scattering loss; while XPS roughens the surface and causes light scattering loss.

LSPR measurement of the sample modified by silicon

The glass substrate implanted with silicon was used for LSPR measurements. In this experiment, polystyrene nanospheres of 170 nm in diameter were dispersed on the glass sample with the process of

PDDA treatment, then 30 nm of gold was thermally evaporated onto the nanospheres at an oblique angle of 70°. After gold evaporation, the SEM image of the sample is as shown in Fig. 5a. The gold evaporated onto the nanospheres forms the 3D nanostructures for LSPR detection, and their top and side views of the gold profiles are simulated in the insets.
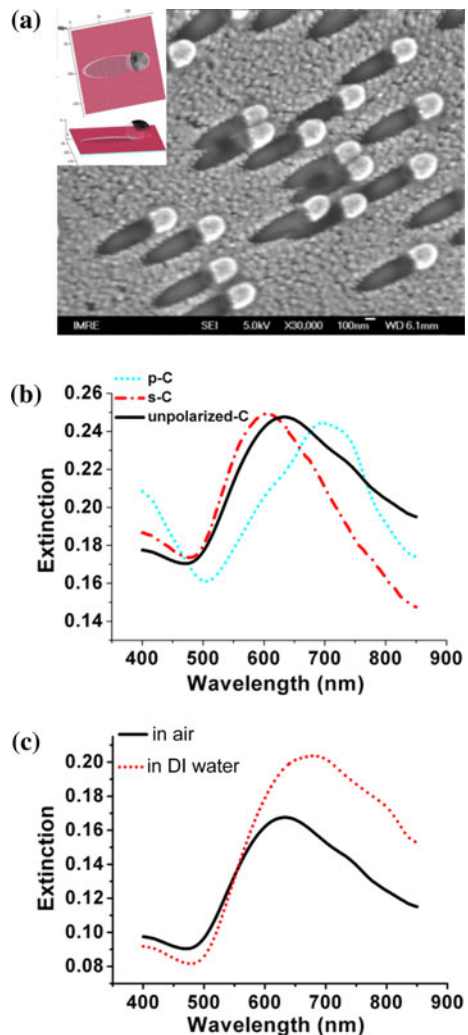

Fig. 5 LSPR spectra of the gold nanostructures fabricated by evaporating 30 nm of gold onto 170 nm diameter polystyrene nanospheres at 70°. **a** demonstrates the gold nanostructures on the substrate, with *insets* show the simulated profile of the gold nanostructures; **b** shows that the LSPR spectrum for unpolarized light is the sum of the two spectra taken when the light polarization is perpendicular (p-C) or parallel (s-C) to the gold evaporation direction; **c** presents the LSPR spectra in air and water for unpolarized light, which indicate a LSPR sensitivity of 242 nm/RIU

This kind of nanostructures is asymmetric and thus the LSPR signal is polarization dependent. Figure 5b presents their LSPR spectra measured in air by the Ocean Optics spectrometer, when the light is polarized or unpolarized. When the polarization of the light is perpendicular to the gold evaporation direction, the light is polarized along the longer side of the 3D nanostructures on the nanospheres, longitudinal plasmon resonance peak at the wavelength of 730 nm is excited; when the polarization of the light is parallel to the gold evaporation direction, the transverse plasmon resonance peak at the wavelength of 590 nm is excited. This polarization dependence of the LSPR resonance peak might be related with the distance between the two ends of the nanostructures for the light to rebound back and forth when oscillating. This phenomenon is similar to the long and short LSPR wavelength peaks reported in gold nanorods (Van der Zande et al. 1997) and nanocrescents (Bukasov and Shumaker-Parry 2007; Rochholz et al. 2007; Shumaker-Parry et al. 2005). For LSPR sensing, any one of these three spectra can be used independently based on the preferred LSPR peak wavelength for a specific application, and the unpolarized LSPR spectrum is the sum of the two spectra measured with orthogonally polarized light beams. When the adjacent medium of these gold nanostructures is changed from air to water, as plotted in Fig. 5c, the LSPR spectra for these two media taken with unpolarized light render a sensitivity of 242 nm/RIU, where RIU is the refractive index unit. This LSPR sensitivity for bulk reflective index variation is compatible to the silver nanotriangles fabricated with closely packed nanosphere lithography in Northwestern University (Zhao et al. 2006), which yielded a sensitivity of 200 nm/RIU.

It is worth noting that the LSPR sensitivity is highly related with the shape and size of the gold nanoparticles. When the thickness of the gold evaporation in Fig. 5 is increased to 50 nm, the LSPR peak is red-shifted and broadened, while presents a higher refractive index sensitivity of 317 nm/RIU, as presented in Fig. 4 of the article published by Zhou et al. (2009). When the nanospheres were burnt up at a high temperature in an oven (350 °C for 90 min) as the SEM picture shown in Fig. 6a, the LSPR peak is blue-shifted with line-width reduced in Fig. 6b, and yields a lower sensitivity of 170 nm/RIU. This is in accordance with the fact that the LSPR sensitivity is
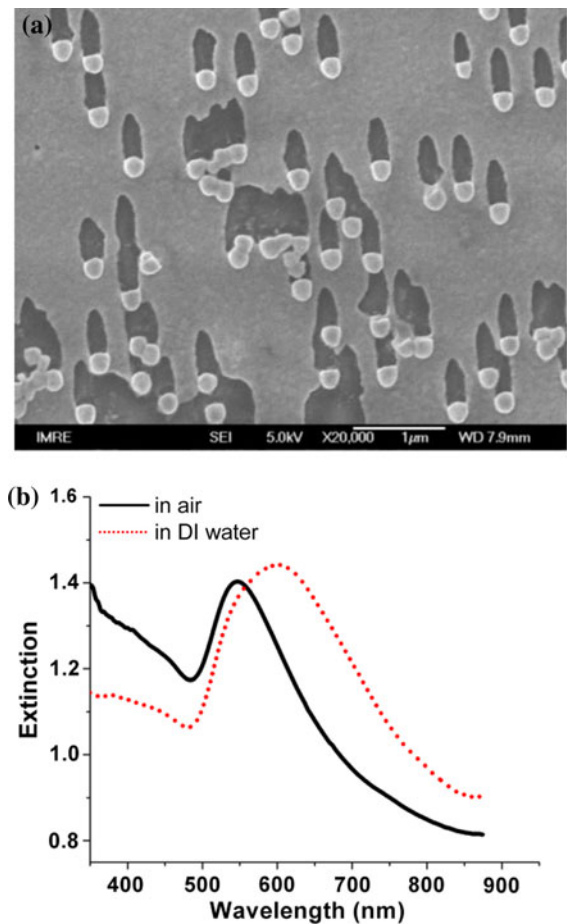

Fig. 6 LSPR spectra of the same gold nanostructures as those in Fig. 5, but with nanospheres burnt out. **a** shows the SEM image, and **b** shows their LSPR spectra in air and water

higher for a peak at longer wavelength (Bukasov and Shumaker-Parry 2007).

Besides the LSPR experiments reported in this article, this nanosphere dispersion method has also been employed for the investigation of gold nanoholes (Xiang et al. 2010) and wet etching of gold nanostructures in dispersed nanosphere lithography (Zhou et al. 2010), thus it is regarded as a practical tool for LSPR applications.

Conclusion

This article investigated in detail on dispersing the nanospheres on a large glass substrate through low dose ion implantation. This method introduces no optical loss to the optical transmission of the glass, and

different kinds of ions can be employed to disperse the nanospheres on a large glass area. Among these ions, silicon is the most efficient, as the glass surface involves directly implanted silicon in addition to the silicon induced by ion bombardment.

By evaporating 30 nm of gold at 70° onto the dispersed nanospheres on the glass substrate, LSPR measurement with bulk refractive index sensitivity of 242 nm/RIU was obtained, however, the LSPR spectrum and its sensitivity are intrinsically sensitive to many factors such as the thickness of the gold, size, and existence of the nanospheres. Besides the nanostructures fabricated in this article for LSPR demonstration, dispersed nanospheres on the glass substrate can also be used to acquire other kinds of gold nanostructures for LSPR, such as nanocrescents obtained by etching the gold film, or nanoholes obtained by removing the nanospheres. In general, this article facilitates the mass and inexpensive fabrication of metal nanostructures in a large glass substrate by dispersed nanosphere lithography, and it is expected to have wider applications on plasmonics or metamaterials.

References

Bukasov R, Shumaker-Parry JS (2007) Highly tunable infrared extinction properties of gold nanocrescents. Nano Lett 7:1113–1118

Endo T, Kerman K, Nagatani N, Takamura Y, Tamiya E (2005) Label-free detection of peptide nucleic acid—DNA hybridization using localized surface plasmon resonance based optical biosensor. Anal Chem 77:6976–6984

Fredriksson H, Alaverdyan Y, Dmitriev A, Langhammer C, Sutherland DS, Zäch M, Kasemo B (2007) Hole-mask colloidal lithography. Adv Mater 19:4297–4302

Gao D, Chen W, Mulchandani A, Schultz JS (2007) Detection of tumor markers based on extinction spectra of visible light passing through gold nanoholes. Appl Phys Lett 90:073901

Hanarp P, Sutherland DS, Gold J, Kasemo B (2003) Control of nanoparticle film structure for colloidal lithography. Colloid Surface A 214:23–36

Homola J (2003) Present and future of surface plasmon resonance biosensors. Anal Bioanal Chem 377:528–539

Homola J, Yee SS, Gauglitz G (1999) Surface plasmon resonance sensors: review. Sens Actuator B Chem 54:3–15

Li Y, Pan J, Zhan P, Zhu S, Ming N, Wang Z, Han W, Jiang X, Zi J (2010) Surface plasmon coupling enhanced dielectric environment sensitivity in a quasi-three-dimensional metallic nanohole array. Opt Express 18:3546–3555

Prikulis J, Hanarp P, Olofsson L, Sutherland D, Käll M (2004) Optical spectroscopy of nanometric holes in thin gold films. Nano Lett 4:1003–1007

Rochholz H, Bocchlo N, Kreiter M (2007) Tuning resonances on crescent-shaped noble-metal nanoparticles. New J Phys 9:53

Shumaker-Parry JS, Rochholz H, Kreiter M (2005) Fabrication of crescent-shaped optical antennas. Adv Mater 17:2131–2134

Van der Zande BMI, Bohomer MR, Fokkink LGJ, Schoneberg C (1997) Aqueous gold sols of rod-shaped particles. J Phys Chem 101:852–854

Willets KA, Duyne RPV (2007) Localized surface plasmon resonance spectroscopy and sensing. Annu Rev Phys Chem 58:267–297

Xiang G, Zhang N, Zhou X (2010) Localized surface plasmon resonance biosensing with large area of gold nanoholes fabricated by nanosphere lithography. Nanoscale Res Lett 5:818–822

Yang S-M, Jang SG, Choi D-G, Kim S, Yu HK (2006) Nanomachining by colloidal lithography. Small 2:458–475

Zhang G, Wang D, Mohwald H (2007) Ordered binary arrays of Au nanoparticles derived from colloidal lithography. Nano Lett 7:127–132

Zhao J, Zhang X, Yonzon C, Haes AJ, Duyne RPV (2006) Localized surface plasmon resonance biosensors. Nanomedicine 1:219–228

Zhou X, Virasawmy S, Knoll W, Liu KY, Tse MS, Yen LW (2008) Fabrication of gold nanocrescents by angle deposition with nanosphere lithography for LSPR applications. J Nanosci Nanotechnol 8:3369–3378

Zhou X, Zhang N, Liu KY, Tan C, Knoll W (2009) Dispersion of nanospheres on large glass substrate by amorphous or polycrystalline silicon deposition for localized surface plasmon resonance. J Nanopart Res 11:2061–2069

Zhou X, Zhang N, Tan C (2010) Profile prediction and fabrication of wet etched gold nanostructures for localized surface plasmon resonance. Nanoscale Res Lett 5:344–352